The C-Terminal Aqueous-Exposed Domain of the 45 kDa Subunit of the Particulate Methane Monooxygenase in Methylococcus capsulatus (Bath) Is a Cu(I) Sponge †

ARTICLE *in* BIOCHEMISTRY · JANUARY 2008

Impact Factor: 3.02 · DOI: 10.1021/bi700883g · Source: PubMed

10 AUTHORS, INCLUDING:

Steve S-F Yu
Academia Sinica
50 PUBLICATIONS **835** CITATIONS
SEE PROFILE

Chien-Hung Lai
Taipei Medical University
26 PUBLICATIONS **213** CITATIONS
SEE PROFILE

Kelvin H.-C. Chen
National Pingtung University
18 PUBLICATIONS **332** CITATIONS
SEE PROFILE

Sunney I Chan
Academia Sinica
388 PUBLICATIONS **11,302** CITATIONS
SEE PROFILE

The C-Terminal Aqueous-Exposed Domain of the 45 kDa Subunit of the Particulate Methane Monooxygenase in *Methylococcus capsulatus* (Bath) Is a Cu(I) Sponge[†]

Steve S.-F. Yu,*[,‡,§] Cheng-Zhi Ji,[‡,§] Ya Ping Wu,[‡] Tsu-Lin Lee,[‡] Chien-Hung Lai,[‡] Su-Ching Lin,[‡] Zong-Lin Yang,[‡] Vincent C.-C. Wang,[‡] Kelvin H.-C. Chen,[‡] and Sunney I. Chan[‡]

Institute of Chemistry, Academia Sinica, Nangang, Taipei 115, Taiwan, and Department of Chemistry, National Cheng-Kung University, Tainan 701, Taiwan

Received May 10, 2007; Revised Manuscript Received September 25, 2007

ABSTRACT: The crystal structure of the particulate methane monooxygenase (pMMO) from *Methylococcus capsulatus* (Bath) has been reported recently [Lieberman, R. L., and Rosenzweig, A. C. (2005) Crystal structure of a membrane-bound metalloenzyme that catalyses the biological oxidation of methane, *Nature 434*, 177−182]. Subsequent work has shown that the preparation on which the X-ray analysis is based might be missing many of the important metal cofactors, including the putative trinuclear copper cluster at the active site as well as ca. 10 copper ions (E-clusters) that have been proposed to serve as a buffer of reducing equivalents to re-reduce the copper atoms at the active site following the catalytic chemistry [Chan, S. I., Wang, V. C.-C., Lai, J. C.-H., Yu, S. S.-F., Chen, P. P.-Y., Chen, K. H.-C., Chen, C.-L., and Chan, M. K. (2007) Redox potentiometry studies of particulate methane monooxygenase: Support for a trinuclear copper cluster active site, *Angew. Chem., Int. Ed. 46*, 1992−1994]. Since the aqueous-exposed domains of the 45 kDa subunit (PmoB) have been suggested to be the putative binding domains for the E-cluster copper ions, we have cloned and overexpressed in *Escherichia coli* the two aqueous-exposed subdomains toward the N- and C-termini of the subunit: the N-terminal subdomain (residues 54−178) and the C-terminal subdomain (residues 257−394 and 282−414). The recombinant C-terminal water-exposed subdomain is shown to behave like a Cu(I) sponge, taking up to ca. 10 Cu(I) ions cooperatively when cupric ions are added to the protein fragment in the presence of dithiothreitol or ascorbate. In addition, circular dichroism measurements reveal that the C-terminal subdomain folds into a β-sheet structure in the presence of Cu(I). The propensity for the C-terminal subdomain to bind Cu(I) is consistent with the high redox potential(s) determined for the E-cluster copper ions in the pMMO. These properties of the E-clusters are in accordance with the function proposed for these copper ions in the turnover cycle of the enzyme.

The conversion of methane to methanol is a difficult process industrially (*1*). However, two methane monooxygenases (MMOs) are found in nature that catalyze this conversion efficiently under ambient conditions of temperature and pressure (*2*−*12*). The particulate methane monooxygenase (pMMO)[1] is a multicopper protein found in the plasma membrane of all methanotropic bacteria (*2*, *4*, *5*, *13*). The soluble methane monooxygenase (sMMO) is expressed in certain strains of methanotrophic bacteria under low copper to biomass conditions. The hydroxylase component of the sMMO is a non-heme diiron enzyme (*14*, *15*). Both MMOs use metal clusters to mediate the controlled oxidation of the alkane.

The pMMO consists of three subunits: PmoA (28 kDa), PmoB (45 kDa), and PmoC (29 kDa) (*13*, *16*). On the basis of the work from the Chan laboratory, ca. 15 copper ions are associated with the enzyme (*3*, *13*): a trinuclear copper cluster and three additional copper ions (the dinuclear copper cluster and the mononuclear copper ion observed in the

[†] This work was supported by Academia Sinica and grants from the National Science Council of the Republic China (NSC 93-2113-M-001-032 and -033).

* To whom correspondence should be addressed. Phone: (886)-2-27898650. Fax: (886)-2-27831237. E-mail: sfyu@chem.sinica.edu.tw.

[‡] Academia Sinica.

[§] National Cheng-Kung University.

[1] Abbreviations: AA spectroscopy, atomic absorption spectroscopy; BCW1, His-tagged C-terminal subdomain of the PmoB subunit containing amino acid residues 257−394; BCW2, GST-tagged C-terminal subdomain of the PmoB subunit containing amino acid residues 282−414; BNW1, His-tagged N-terminal subdomain of the PmoB subunit containing amino acid residues 54−178; C-clusters, the catalytic copper ions of pMMO that participate in dioxygen chemistry and alkane hydroxylation; CD spectroscopy, circular dichroism spectroscopy; DelPhi, program that calculates electrostatic properties for charged molecules; DTT, dithiothreitol; *E. coli*, *Escherichia coli*; E-clusters, the copper ions of pMMO that serve as a buffer of reducing equivalents to re-reduce the C-clusters after the catalytic chemistry; EPR, electron paramagnetic resonance; GST, glutathione S-transferase; His, histidine; IMAC, immobilized metal-chelate affinity chromatography; IPTG, isopropyl β-D-thiogalactopyranoside; LB medium, Luria−Bertani medium; *M. capsulatus* (Bath), *Methylococcus capsulatus* (Bath); MALDI-TOF, matrix-assisted laser desorption/ionization time-of-flight; MREs, mean residue ellipticities; NADH, nicotinamide adenine dinucleotide; NMS medium, nitrate mineral salt medium; PDB, Protein Data Bank; pMMO, particulate methane monooxygenase; PMSF, phenylmethanesulfonyl fluoride; SDS−PAGE, sodium dodecyl sulfate−polyacrylamide gel electrophoresis; sMMO, soluble methane monooxygenase; TMHMM, transmembrane topology with a hidden Markov model.

10.1021/bi700883g CCC: $37.00
Published on Web 11/07/2007

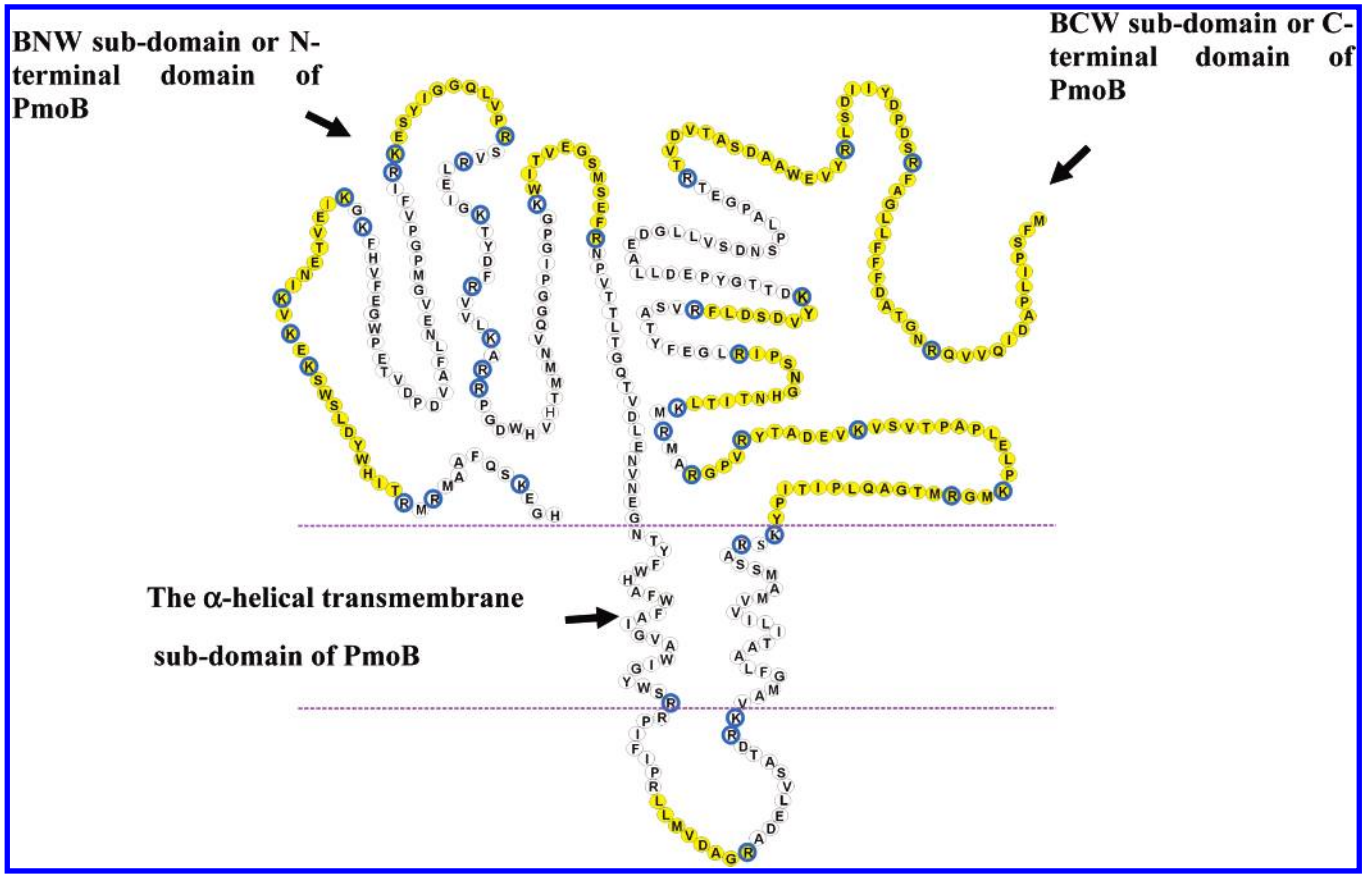

FIGURE 1: Topological arrangement of PmoB.

crystal structure (vide infra) (*7*)) have been implicated in the dioxygen chemistry (*3*, *17*−*19*) as well as the alkane hydroxylation, and the remaining copper ions are proposed to be sequestered into a Cu(I) domain to provide a reservoir of reducing equivalents to re-reduce the copper ions at the active site after the oxidative phase of the turnover (*20*, *21*). The six copper ions that mediate the catalytic chemistry have been referred to as C-clusters, and the reservoir of Cu(I) ions that serve as the buffer of reducing equivalents have been dubbed E-clusters (*20*). Preliminary evidence suggests that the E-clusters might be located in the exposed domains of the protein at the membrane−water interface (*21*, *22*), whereas the C-cluster copper ions are embedded in the transmembrane domain (*7*, *17*). The enzyme is functional only when all the copper ions are reduced. There is no direct evidence that there are any iron or zinc ions associated with the active purified protein (*3*, *13*, *16*). However, the number and type of the copper cofactors remain controversial despite years of intense activity (*2*, *4*, *13*, *23*, *24*). Whether iron cofactors might also be involved in the function of the enzyme is still not fully settled (*2*, *4*, *13*, *23*, *24*).

Recently, the three-dimensional crystal structure of pMMO from *Methylococcus capsulatus* (Bath) has been reported by Lieberman and Rosenzweig (*7*). The protein−detergent complex crystallizes as an $(\alpha\beta\gamma)_3$ trimer. The X-ray structure confirms the 15 putative transmembrane α-helices predicted earlier by amino acid sequence analysis of the three pMMO subunits (28, 45, and 29 kDa) using the program TMHMM (transmembrane topology with a hidden Markov model) and the three-dimensional folding of the subunits modeled by the protein fold recognition server based on the 3D position-specific scoring matrix method (*3*, *22*). The amino acid residues of both PmoC and PmoA are embedded as α-helices (seven segments for PmoA and six for PmoC) in the transmembrane region as predicted; the PmoB subunit consists of only two transmembrane α-helices, but with two water-exposed domains, one at the N-terminus and the other toward the C-terminus (Figure 1). These water-exposed domains of PmoB (residues 33−186 and residues 254−414) have previously been implicated by the hydrophilic peptides excised in in situ membrane trypsin digest experiments and identified by peptide mass fingerprinting by MALDI-TOF mass spectrometry (*22*). An interesting prediction of the theoretical modeling is that the C-terminal water-exposed sequence (N255−M414) of PmoB matched the β-sheet structure of the multidomain cupredoxins. This structural feature is also borne out by the X-ray structure.

According to the X-ray structure of pMMO from *M. capsulatus* (Bath), the three-dimensional structure of the enzyme contains only one mononuclear copper center, one dinuclear copper cluster, and one zinc ion as cofactors per $\alpha\beta\gamma$ monomer; in addition, five additional zinc ions are associated with the trimeric structure (*7*). The zinc ions are artifacts of crystallizing the protein from $Zn(OAc)_2$ solution. There is no evidence of any iron in the structure. On the other hand, the enzyme preparation on which the X-ray analysis is based does not possess biochemical activity (*7*, *17*). Active preparations of pMMO have been shown to contain many more than three copper ions per protein, whether the enzyme activity is assayed using NADH or duroquinol as the reductant (*2*−*4*, *6*, *13*, *16*). Subsequent work has shown that the Lieberman−Rosenszweig preparation is missing many of the important copper cofactors (*17*). It is well-known that pMMO is difficult to isolate and purify,

and many of the copper ions are typically lost during the harsh conditions commonly employed to purify membrane proteins (*16*, *25*).

As an initial step toward reconciling the biochemical/biophysical data with the X-ray structure, we have applied molecular cloning techniques to overexpress the two aqueous-exposed subdomains of PmoB (45 kDa subunit) in *Escherichia coli*. Both the N-terminal subdomain (residues 54−178) and the C-terminal subdomain (residues 257−394 and 282−414) were overproduced as His-tagged and glutathione S-transferase (GST)-fused recombinants, and the purified recombinant protein fragments were examined for their affinity toward copper ions, as the GST-fused protein, in the His-tagged form or with the His tag(s) removed. Since these regions of the three-dimensional fold are judiciously located for NADH or other water-soluble reductants to access the E-clusters to replenish the reducing equivalents after these copper ions have become oxidized by turnover at the active site, they offer the best candidates for the location of the E-cluster domain(s).

MATERIALS AND METHODS

Bacterial Strains, Plasmids, and Growth Conditions. E. coli strains DH5α (Yeastern Biotech) and BL21 (DE3) (Novagen) and the plasmids yT&A (Yeastern Biotech), pET-16b (Novagen), and pGEX-5X-1 (GE Healthcare) were used for DNA manipulations and protein overexpression in this study. They were grown in LB medium in the presence of appropriate amounts of ampicillin (50 μg/mL). The growth of *M. capsulatus* (Bath) (ATCC 33009) was carried out following the procedure of Chan et al. (*13*, *16*) on nitrate mineral salt medium (NMS buffer, ATCC buffer) in a 5 L fermentor with or without the addition of $CuSO_4$ (30 μM concentration) and by purging with a 50%:50% (v/v) CH_4:air ratio. A Bioflo 3000 fermentor was adapted with a hollow-fiber membrane bioreactor to control the copper ion concentration rigorously and to adjust the $CuSO_4$ concentration in suitable increments. This method of culturing the bacteria yields high levels of biomass (70−80%) and overproduced pMMO (80−90% of the total membrane proteins) in the intra cytoplasmic membranes of the cell. pMMO-enriched membranes were isolated and purified as described previously (*13*, *16*).

Preparation of Genomic DNA from M. capsulatus (Bath). The genomic DNA preparation was performed by a genomic extraction kit (Protech Pharmaceutical Co.). *M. capsulatus* (Bath) cell pellets (0.50 g) were resuspended with 200 μL of lysozyme solution (20 mg/mL) at 37 °C for 1.5 h, and the extraction buffer (350 μL) and 4.0 μL of proteinase K reaction buffer (23 mg/mL) were added at 56 °C for 3 h. DNA binding buffer solution was then added to the mixture at the same temperature, and the reaction conditions were sustained until all the cell debris had been completely lysed. To remove the residual proteins, the solution was washed with 1× phenol/chloroform/isoamyl alcohol (25:24:1) and 2× chloroform/isoamyl alcohol (24:1). The supernatant was transferred to a fresh microcentrifuge tube, and 0.6 volume of 2-propanol was added to precipitate the DNA.

Insertion of PmoB Aqueous-Domain-Encoded DNAs into the pET16b-Based Protein Overexpression Vector. For amplification of His-tagged fused pMMO aqueous-exposed subdomains of PmoB located at residues 54−178 and 257−394, polymerase chain reactions (PCRs) were carried out using (i) pmoBw1F160 (5′-TTGGTCGAAAGAGAAAGTC-3′), (ii) pmoBw1R549 (5′-GTAGTTCTCCAGGATCCAC-3′), (iii) pmoBw2F769 (5′-GGATCCAAAGTACCCGAT-CACCATC-3′), and (iv) pmoBw2R1182 (5′-TAAGAAGA-AGAACAGCAGACC-3′) as the primers and *M. capsulatus* (Bath) genomic DNA as the template. The resultant amplified PCR products were ligated to yT&A vectors (Yestern Biotech) first and constructed as yT&A2676 plasmids. yT&A2676 plasmids were then digested by a restriction enzyme, *Bam*H1 (New England Biolabs), and subsequently ligated to the *Bam*H1-linearized pET16b. DNA sequencing analyses mediated by the T7 promoter primer (5′-TAATAC-GACTCACTATAGGG-3′) were exploited to identify the plasmids pETB160 and pETB769 carrying the open reading frames of PmoB 54−178 and 257−394 residues, together with the mutations V81A P84L H137Y E160D and V322E E343D, respectively.

Insertion of PmoB Aqueous-Domain-Encoded DNAs into pGEX-5X-1-Based Protein Overexpression Vector. For amplification of GST-fused PmoB aqueous-exposed domain located at residues 282−414, we followed the same procedure as for the His-tag-encoded vector of pET16b described above. Two oligo(deoxyribonucleotide) primers, (i) pmoBw3F842 (5′-GGATCCAAAGTACCCGATCACCATC-3′) and (ii) pmoBw3R1245 (5′-TAAGAAGAAGAACAGCAGACC-3′), were used to synthesize the *pmoB* aqueous-domain gene from *M. capsulatus* (Bath) genomic DNA. These 403 bp encoded fragments were subsequently ligated to the *Bam*H1 sites of pGEX-5X-1 to obtain the plasmid pGEXB842 carrying the open reading frames for the gene of PmoB 282−414 residues for protein expression.

His-Tagged and GST-Fused PmoB Aqueous-Domain Induction into E. coli BL21 (DE3). Single colonies of pETB- and pGEXB-transformed bacteria strains were grown overnight in 3.0 mL of LB buffer with ampicillin (50 mg/mL) at 37 °C. For 300 mL growth induction, 3 mL of overnight culture was added to the LB medium in a 2 L Erlenmeyer flask, and the bacteria were grown at 37 °C until the turbidity of the culture reached an OD_{600} of 0.8. At this point, 0.6 mM isopropyl β-D-thiogalactopyranoside (IPTG) was added, and the temperature was lowered to 30 °C. After another 2.0 h of growth, we harvested the bacterial strains that contained the recombinant proteins for purification and identification.

For large-scale recombinant protein expression, we carried out the bacteria growth in a 10 L FB10 fermentor (Firstek Scientific, Taiwan). A 50−100 mL portion of LB overnight growth medium carrying the engineered vectors was inoculated in 3.0 L of ampicillin containing 1× LB medium in a 10 L fermentor vessel. During the stage of bacteria cell differentiation, we maintained the growth temperature at 37 °C and the pH values in the range of 6.9−7.1. We also adjusted the air-feeding rate to 1.0 L/min and the agitation speed to 500 rpm. After 2.0 h of cell growth when the OD_{600} of the cells reached 2.0−3.0, we added another 4.0 L of 2.5× LB medium to the fermentor vessel. The agitation speed was maintained at 500 rpm, and the bacteria growth was continued for another 1.5 h. The temperature was then adjusted to 37 °C, 0.6 mM IPTG was added to the fermentor vessel, and the culturing was continued until the cell density

reached the late-log phase. After 1.0−1.5 h, we harvested the cell culture containing the expressed recombinant proteins. Typically, yields of 7.0−10 g/L wet cells were obtained.

SDS−PAGE Analysis of the Overexpressed Proteins. For the analysis of the protein expression profiles, 1 mL overnight growths were collected, centrifuged at 12 000 rpm, and resuspended in 5.0 mL of 20 mM Tris−HCl buffer, and the solutions were sonicated for 10 min. The sonicated mixtures were then centrifuged at 12000*g* for 20 min. After separation of the pellet from the supernatant, 4 mL of a 20 mM Tris−HCl (pH 8.0) solution was added. Finally, 3.0 μL aliquot solutions of the supernatant and pellet, respectively, were mixed with 2.0 μL of pH 8.0 Tris−HCl buffer and 5.0 μL of 2× sample loading buffer, and the proteins were subjected to SDS−PAGE gel electrophoresis.

Purification of Recombinant-DNA Overexpressed Proteins. To a 20 g wet mass of IPTG-induced bacteria was added 20 mM pH 8.0 Tris−HCl. After addition of 10 mg of DNase I, the cell mixture was lysed by a French pressure cell at 1280 psi/cm^2. A 15 mL portion of a 1.0 mM PMSF solution was then added to the lysis solution, and any remnant cells were subjected to lysis by the French pressure cell again. After centrifugation at a speed of 8000 rpm at 4 °C for 30 min, the solution was separated into supernatant and pellet.

If the overexpressed proteins appeared to be water-soluble, the supernatant was subjected to ultracentrifugation at 36 000 rpm for 1.0 h and filtered through a 0.45 μm membrane (Millipore). For overexpressed proteins that ended up in inclusion bodies, 4 M urea was added to solubilize the proteins for 30 min at room temperature. The solubilized proteins were then ultracentrifuged for 1.0 h and filtered through a 0.45 μm membrane.

For purification of the His-tag-containing solubilized proteins, an immobilized metal-chelate affinity chromatography (IMAC) column was charged with 0.20 M nickel sulfate solution. After ultracentrifugation (36 000 rpm, 1.0 h), the supernatant was applied to the Ni^{2+}-charged chelating Sepharose fast flow column (GE Healthcare). The protein was eluted by the elution buffer (20 mM Tris−HCl, pH 8.0, 0.5 M NaCl, 4 M urea) with increments of imidazole concentrations (50, 100, 200, 300, and 500 mM) for every 5× column volume.

To purify the solubilized GST-fused proteins, the supernatant was injected onto a glutathione Sepharose chromatography column. To obtain the proteins, the affinity column was eluted with 5× column volumes of binding buffer (140 mM NaCl, 2.7 mM KCl, 10 mM Na_2PO_4, 1.8 mM KH_2PO_4, and 50 mM Tris−HCl in pH 7.3 phosphate buffer), elution buffer (10 mM reduced glutathione and 1 mM dithiothreitol (DTT) in pH 8.0 50 mM Tris−HCl), washing buffer (15 mM reduced glutathione and 1 mM DTT), doubly distilled water, 1% Triton X-100, and 6.0 M guanidine−HCl, respectively. Finally, the proteins were purified by equilibrium dialysis using 10 000 MW cutoff dialysis membranes against 3.0 L of pH 7.3 Tris−HCl buffer three times. They were then viewed by one-dimensional SDS−PAGE gel electrophoresis.

Removal of His Tag from the pET-Based Overexpression Proteins. By use of the Factor Xa kits from Novagen, the His tags were removed from the overexpressed proteins. Possible interferences from the His-tagged residues in the characterization of the proteins were then ascertained.

To 10 μg of fusion proteins in a 45 μL solution were added 1 μL of 0.3 U/μL Factor Xa solution and 5 μL of 10× Factor Xa cleavage solution. The cleavage reaction was allowed to proceed for 1.0 h at 20 °C. Sufficient amounts of Xarrest agarose were then added to the reaction mixture to remove the Factor Xa. After centrifugation at 1000*g* for 5 min, the supernatant was decanted and the filtrate was washed with 1× capture solution by centrifugation at 1000*g* for another 5 min. Upon the addition of a second aliquot of 1× capture solution and following standing for 5 min, the reaction mixture was centrifuged at 1000*g* again for 5 min to separate the solution from the agarose. The cleaved proteins were then purified by flow-through on a Ni^{2+}-charged chelating Sepharose fast flow column, which removed remnants of the uncleaved proteins.

CD Spectroscopy. The overexpressed proteins with and without metal ions were dissolved in 20 mM pH 8.0 Tris−HCl buffer at room temperature. CD spectra were recorded in a π* CD spectrometer (Applied Photophysics, Surrey, U.K.) over the spectral range between 200 and 300 nm at room temperature in a 1 mm cell using a volume of 400 μL of solution. A scan interval of 1 nm with an integration of 200 000 points was used. The spectrum of the same buffer was collected as a baseline and subtracted automatically. The CD spectra obtained were normalized and presented in units of mean residue ellipticities (MREs; (deg·cm^2)/(dmol·residue)).

Binding of Metal Ions to the Recombinant Proteins. Method 1. The interactions of Cu(I) and Cu(II) ions with the PmoB aqueous-exposed subdomains were examined. To each of the recombinant proteins in pH 8.0 Tris−HCl buffer (20 mM), 10−100 equiv of $CuSO_4$ solution was added. The final concentrations of the overexpressed proteins were typically on the order of 20 μM. The affinity of the recombinant proteins for Cu(I) was studied by the addition of DTT to solutions containing $CuSO_4$ at 2× metal ion concentration. Quantification of the binding of the reduced copper ions to the PmoB aqueous subdomains was carried out by dialysis using a 10 000 MW cutoff dialysis membrane against a buffer solution of 1.0 mM DTT, 20 mM Tris−HCl, and 1.0 mM NaCl. During the "2× dialysis" the bulk of the Cu(I) incorporated into the proteins remained bound and was determined by atomic absorption (AA) measurements as follows. The recombinant protein samples (0.2 mL) complexed with metal ions were dissolved in 4.8 mL of saturated 65% HNO_3 solution (suprapure grade, Merck) and digested at 180 °C in a MARS5 microwave digestion system (CEM Inc.). The digested samples were then diluted with appropriate amounts of doubly distilled water (Millipore) prior to copper analysis. The copper concentrations of the samples were determined relative to that of a standard solution of $Cu(NO_3)_2$ in 0.10 N HNO_3. A solution of 0.10 N HNO_3 in distilled water was used as the copper-free control. Protein concentration after dialysis was measured by the Bradford method (Biorad) using bovine serum albumin as a standard (*26*). The measured amount of Cu(I) bound was divided by the protein present to give the average Cu(I) content per unit of protein (υ). The free "Cu(I)" in equilibrium with the protein−Cu(I) complex was determined by subtracting the amount of Cu(I) bound to the protein from

the concentration of the Cu(I) formed by DTT reduction of the total $CuSO_4$ initially added to the protein sample. Since the initial Cu(II) concentration was in large excess of the protein concentration, the free copper ion concentration at equilibrium differed by no more than 50% from the initial concentration even with appreciable copper binding to the protein in these experiments. The measured Cu(I) content per unit of protein (υ) and the free Cu(I) concentration reported as [Cu^+] are the averages of three separate determinations.

Method 2. The method of Jensen et al. (*27*) was also used to study the binding of Cu(I) to the recombinant BCW1 preparation. An aliquot of $CuCl_2$ solution in 0.5 M NaCl, 10 mM ascorbate, 50 mM Tris−HCl, pH 7.4, was added to the recombinant protein. The concentration of Cu(I) was varied from 0 to 1.0 mM, and the concentration of the overexpressed protein was maintained at 20 μM. The amount of Cu(I) complexed to the recombinant protein was determined as follows. To each aliquot was then added 0.060 g of the cation-chelating resin Chelex 100 to remove unbound or nonspecifically bound copper in the protein solutions. After 1.0 h of incubation, the resin was removed by centrifugation and the supernatant was analyzed for protein and copper content. The protein concentration was measured by the Bradford method (Biorad) using bovine serum albumin as a standard (*26*). The Cu(I) concentration was determined spectrophotometrically using bicinchoninic acid (BCA) (disodium salt, Sigma Inc.). A large amount of BCA (20 mM) was added to the protein sample to shift the Cu(I) binding equilibrium from the protein (20 μM) to BCA. Under these conditions, we have shown that all the Cu(I) bound to the protein (up to a concentration of 15 μM) will be stripped off and become bound to the dye. The absorbance of ascorbate-reduced Cu(I) in the presence of BCA followed a linear correlation with Cu(I) concentration in accordance with Beer−Lambert's law in the range 10−100 μM Cu(I) at a wavelength of 562 nm ($r^2 = 0.99$). No chromophoric absorption was observed in the presence of Cu(II), or in the absence of metal ions, upon the addition of BCA. For each individual ascorbate-reduced copper titration, the measured Cu(I) content per unit of protein (υ) represented the average of three separate determinations. As in method 1, the free Cu(I) in equilibrium with the protein−Cu(I) complex was estimated by the concentration of the amount of Cu(I) initially formed by ascorbate reduction minus the concentration of Cu(I) bound. Again, the initial Cu(II) concentration was in large excess of the protein concentration so that the free copper ion concentration at equilibrium differed by less than 50% from the initial concentration.

Analysis of Cu(I)-Binding Data. The Cu(I) binding to the recombinant subdomains was modeled as multiple equilibria within the framework of the Hill model with positive cooperativity (*28*)

$$P + n\mathrm{Cu(I)} \leftrightarrows P{-}\mathrm{Cu(I)}_n$$

with a Cu(I) dissociation constant of K_D

$$K_D{}^n = [P][\mathrm{Cu(I)}]^n/[P{-}\mathrm{Cu(I)}_n]$$

and cooperativity described by the Hill constant α_H, where $1 \leq \alpha_H \leq n$. The Hill plot is given by

$$\ln [\mathrm{Cu(I)}] = -(1/\alpha_H)[\ln[n/\upsilon] - 1] + \ln K_D \quad (1)$$

and the Scatchard plot by

$$\upsilon/[\mathrm{Cu(I)}] = n\{[\mathrm{Cu(I)}]^{(\alpha_H-1)}/K_D{}^{\alpha_H}\}\{1 + \{[\mathrm{Cu(I)}]^{\alpha_H}/K_D{}^{\alpha_H}\} \quad (2)$$

where [Cu(I)] is the concentration of free Cu(I) at equilibrium, υ denotes the average number of moles of Cu(I) bound per mole of the recombinant BCW1, and n is the number of binding sites for Cu(I) in the domain.

Redox Potentiometry. An electrochemical cell was constructed according to the design of Dutton (*29*). Gold electrodes (2 mm in diameter) from CH Instruments were deployed as the working electrodes. The Ag/AgCl electrode was used as a reference. Cell potentials were monitored by a Suntex SP-2000 pH meter.

Potentiometric Titrations. Potentiometric titrations of the pMMO were carried out in the absence of hydrocarbon substrate as follows. pMMO-enriched membranes (0.35−0.5 mM in 5 mL of PIPES buffer) were first flushed with dioxygen for 25 min. The samples were then transferred to the electrochemical cell. Aliquots of 100 μL of different redox mediators, each at a concentration of 2.4 mM, were then added to the solution. The final volume was typically 6 mL, and the final concentration of each mediator was 40 μM.

The following redox mediators were used in the potentiometric titrations (*29*): phenazine methosulfate ($E^{\circ\prime} = +80$ mV), phenosafranin ($E^{\circ\prime} = -252$ mV), anthrax−quinone-2-sulfonic acid ($E^{\circ\prime} = -225$ mV), methylene blue ($E^{\circ\prime} = +21$ mV), neutral red ($E^{\circ\prime} = -340$ mV), 2-hydroxy-1,4-naphthoquinone ($E^{\circ\prime} = -145$ mV), resorufin ($E^{\circ\prime} = -51$ mV), methyl viologen ($E^{\circ\prime} = -430$ mV), benzyl viologen ($E^{\circ\prime} = -311$ mV), and indigo carmine ($E^{\circ\prime} = -125$ mV). All reduction potentials are referred to the standard hydrogen electrode (SHE).

After the sample had been incubated for 25 min, the cell potential of the solution was measured, and a 200 μL solution was transferred from the electrochemical cell to a quartz EPR tube and rapidly chilled for subsequent EPR measurements. All redox titrations and sample transfers were performed in a glovebox (COY Laboratory Products, Inc., Michigan) to avoid complications from further reactions of the protein with dioxygen.

Electron Paramagnetic Resonance. EPR spectra of the various samples were recorded at X-band (9.6 GHz, modulation frequency 100 kHz, and modulation amplitude 5 G) on a Bruker E580 spectrometer equipped with a Bruker dual-mode ER 4116DM cavity. The sample temperature was maintained at 4 or 6 K by using an Oxford Instruments continuous liquid helium cryostat equipped with a turbopump to lower the vapor pressure of the liquid helium. A capillary containing 0.5 mM $CuCl_2$ in 1:1 (v/v) pure water/glycerol was employed as a standard sample for spin counting. EPR spectra of the background were also recorded and subtracted from the sample spectra prior to double integration to determine the Cu(II) concentration in the sample. When the Cu(II) signals monitored were weak due to low concentrations, an EPR spectrum of the membranes was also recorded after complete reduction with dithionite to correct for possible

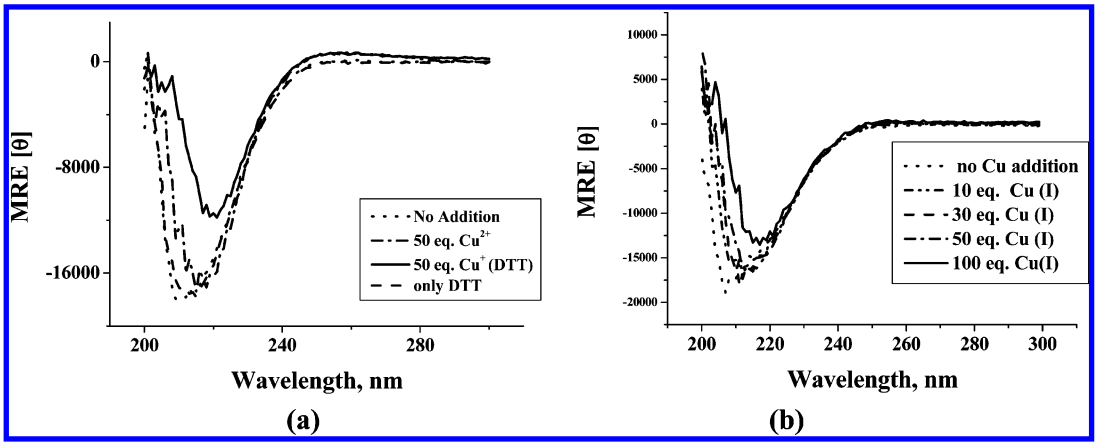

FIGURE 2: CD spectra of the BCW1 V322E E343D subdomain recorded (a) in the absence or presence of Cu(I) or Cu(II) ions and (b) after the addition of varying concentrations of Cu(I) ions produced by reduction of Cu(II) by DTT.

interferences from low levels of background signals arising from the membranes.

RESULTS

Overexpression of the N-Terminal and C-Terminal Subdomains of the PmoB Subunit in E. coli and Structural Characterization by CD in the Absence and Presence of Copper Ions. Toward structural studies of the N-terminal and C-terminal aqueous subdomains of the PmoB subunit and the determination of their affinities toward copper ions, we have cloned and overproduced these subdomains in *E. coli*. These proteins correspond to the two encoded peptides with amino acid residues 54−178 and 257−394 of PmoB, respectively. The pET-based vectors containing each of the two corresponding genes were first transformed into *E. coli* BL21 (DE3) to generate the His-tagged BNW1 V81A P84L H137Y E160D (abbreviated as the polypeptides of the BNW1 domain, residues 54−178, 20 kDa) and the His-tagged BCW1 V322E E343D (abbreviated as the polypeptides of the BCW1 domain, residues 257−394, 18 kDa), respectively. These overexpressed proteins were verified by the encoded DNA sequence of the inserted oligonucleotides as well as their molecular masses from one-dimensional SDS−PAGE gel electrophoresis and MALDI-TOF analysis.

(1) BNW1. The apo-BNW1 was expressed in *E. coli* as an inclusion body. This protein precipitate could be denatured and solubilized in 4.0 M urea and recovered as a folded native structure after 3× dialysis treatments in a 10 000 MW cutoff dialysis membrane against 1.0 L of 1.0 mM DTT, 20 mM Tris−HCl, and 1.0 mM NaCl buffer solution. The poly-His-tagged residues were then removed by Factor Xa. After purification, the CD spectrum of the apo-BNW1 was recorded. This peptide fragment exhibited reasonable water solubility and gave a feature at 222 nm characteristic of β-sheet structure. No obvious conformational change was detected when either Cu(II) or Cu(I), namely, Cu(II) plus DTT, was added to the protein solution. This subdomain readily precipitated upon the addition of either Cu(I) or Cu(II) so that it was not possible to obtain any copper binding data.

(2) BCW1. The apo-BCW1 V322E E343D subdomain was also expressed as an inclusion body. Similar procedures were deployed to denature and recover the protein in its native form. Again, the poly-His tag was removed by Factor Xa protease. The CD spectrum revealed that a substantial proportion of the apo-BCW1 secondary structure was a random coil (Figure 2a). However, upon the addition of 50 equiv of $CuSO_4$ (1 mM) to the peptide solution, some minor conformational changes were observed. The CD spectrum became slightly red-shifted toward that of a β-sheet structure. If, in addition, 100 equiv of DTT was added to reduce the Cu(II) ions to Cu(I), the secondary structure was dramatically shifted to the standard β-sheet, as revealed by CD (Figure 2a). The effects of adding increasing increments of Cu(I) to the protein solution are depicted in Figure 2b. At 100 equiv of Cu(I), the CD minimum had shifted to 218 nm, with the MREs [θ] approaching a value of −12 000 (deg·cm^2)/(dmol·residue) at this wavelength (Figure 2b). In this experiment, we took precautions to ensure that all the Cu(II) in the solution had been totally reduced to Cu(I), as confirmed by the total disappearance of Cu(II) features in the EPR. As additional controls, we also showed that the addition of Cu(II) as well as DTT alone to the recombinant apo-BCW1 V322E E343D subdomain at the aforementioned concentrations did not account for the CD changes observed with Cu(II) + DTT (Figure 2a).

The β-sheet structure of the BCW1 V322E E343D subdomain remained stable upon removal of weakly bound and unbound Cu(I) ions. To demonstrate this, a number of experiments were performed in which varying amounts of $CuSO_4$(aq) ranging from 5 to 100 equiv were added to 20 μM BCW1 V322E E343D in the presence of 2× the corresponding copper ion concentration of DTT. From the CD spectra, it is evident that the conformation of the Cu(I)-enriched BCW1 V322E E343D had converged toward the limiting β-structure after 10−100 equiv of Cu(I) had been added, with the MREs approaching a limiting [θ] = −15 000 to −12 000 (deg·cm^2)/(dmol·residue) over the wavelength span from 210 to 217 nm. When weakly bound or unbound Cu(I) ions were removed from the solution by dialyzing the Cu(I)-enriched BCW1 V322E E343D using dialysis tubing with a 10 000 MW cutoff against 1.0 mM DTT, 20 mM Tris−HCl, and 1.0 mM NaCl buffer solution, and the limiting CD spectrum after dialysis (Figure 3) was compared with the corresponding spectrum before dialysis in each case (Figure 2b), it was apparent that the BCW1 V322E E343D had retained most of its β-sheet structure even after extensive dialysis. Thus, the subdomain has a strong affinity toward Cu(I) ions, and the Cu(I) complex is kinetically stable!

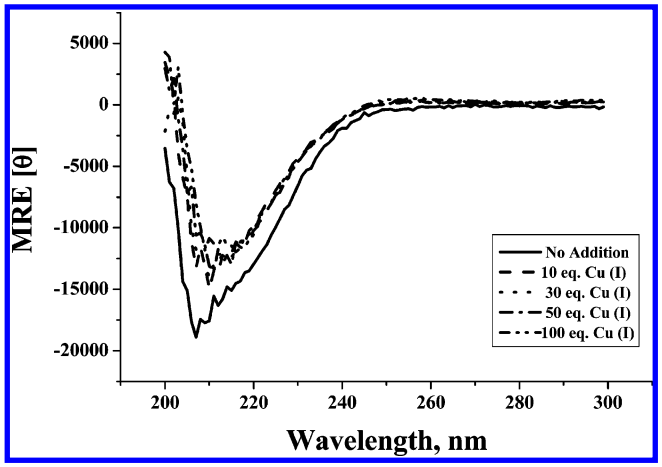

FIGURE 3: CD spectra of the BCW1 V322E E343D subdomain in the presence of varying concentrations of Cu(I) ions produced by reduction of Cu(II) by DTT, after 3× dialysis against 1.0 mM DTT, 20 mM Tris−HCl, and 1.0 mM NaCl buffer solution.

Quantitation of the Cu(I) Binding to Apo-BCW1. To quantify the affinity of the recombinant His-tag-free BCW1 V322E E343D subdomain toward Cu(I), we determined the number of copper ions associated with the subdomain as a function of Cu(II) plus DTT added to the protein solution. The Cu(I) ions were generated using two different reductants: DTT and ascorbate. Since the solubility of Cu(I) in aqueous buffer is low, the conditions of equilibrium binding could only be achieved in the presence of the reductant. The thermodynamic parameters determined for the Cu(I)−protein binding equilibrium would also be dependent on the reductant used, because the thermodynamic activity of the "free" Cu(I) will depend on the extent of interaction between the Cu(I) and the reductant.

(1) DTT as the Reductant. The number of Cu(I) ions bound to the apo-BCW1 was determined as various concentrations of Cu(II) + DTT were added to protein solutions of a defined concentration, and the concentration of unbound reduced copper in equilibrium, in the form of either free Cu(I) or Cu(I) associated with DTT, was also estimated in each case using equilibrium dialysis. The data were then analyzed by the conventional Scatchard and Hill plots (*28*).

Figure 4a depicts the Scatchard plot of υ/[Cu(I)] vs υ, with a maximum of $n(\alpha_H - 1)/\alpha_H$ occurring at $\upsilon = \upsilon_{max}$ and an x intercept at $\upsilon = n$. The Hill plot (Figure 4b) is a ln−ln plot and should be a straight line with a slope of $-1/\alpha_H$ and ln [Cu(I)] equal to ln K_D when the abscissa is set equal to 0. From the curvature of the Scatchard plot, it is immediately apparent that the binding interaction between Cu(I) and BCW1 V322E E343D is cooperative. From the value of υ_{max}, we obtained a Hill constant α_H of ∼3.0, and from the x intercept, the number of binding sites in the BCW1 V322E E343D subdomain can be estimated to be 16 ± 1. From the Hill plot depicted in Figure 4b, we obtained a Hill constant of $\alpha_H = 3.2$ and a dissociation constant K_D of 370 μM. The fractional saturation data are plotted vs [Cu(I)]/K_D in Figure 4c and compared with theoretical curves expected for α_H = 3.0 and 3.2. As expected for cooperative binding, the fractional saturation is not so sensitive to the value of the Hill constant as long as the Cu(I) binding is reasonably cooperative.

In a separate control experiment, 50 equiv of Cu(II) ions was added to a 20 μM apo-BCW1 solution without the addition of DTT, and the number of Cu(II) ions bound to the overexpressed C-terminal subdomain was determined by equilibrium dialysis with a 10 000 MW cutoff membrane against 20 mM Tris−HCl and 1.0 mM NaCl buffer solution. From this experiment, we concluded that there was no substantial Cu(II) ion binding to the recombinant C-terminal aqueous subdomain. The number of Cu(II) ions "bound" per BCW1 subdomain was measured to be 0.36 ± 0.20.

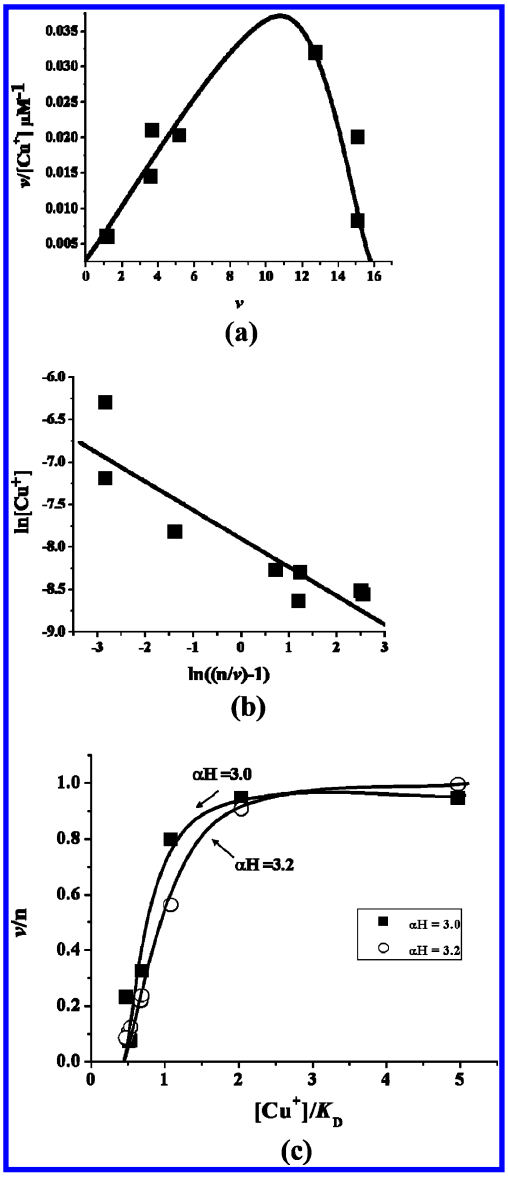

FIGURE 4: (a) Scatchard plot (eq 2) for the binding of DTT-reduced copper ions to apo-BCW1 V322E E343D after removal of the His tag. (b) Linear Hill plot of eq 1. (c) Effect of the Hill constant α_H on the fractional saturation curve and comparison with experiment (○, $\alpha_H = 3.2$; ■, $\alpha_H = 3.0$).

(2) Ascorbate as the Reductant. We have repeated the Cu(I) titration of apo-BCW1 using ascorbate as the reductant to generate Cu(I) from Cu(II). We did not remove the His tag for the titration presented here. We found that it was difficult to maintain the stability of the His-tag-free peptides, and we often observe the fragmentation occurred after the protease digestion. For this reason, the quality of the titration data obtained was better with the His tag intact.

Scatchard and Hill plots of the titration data obtained with the ascorbate/BCA method on the poly-His-tagged recombinant protein are presented in Figure 5. From the Scatchard

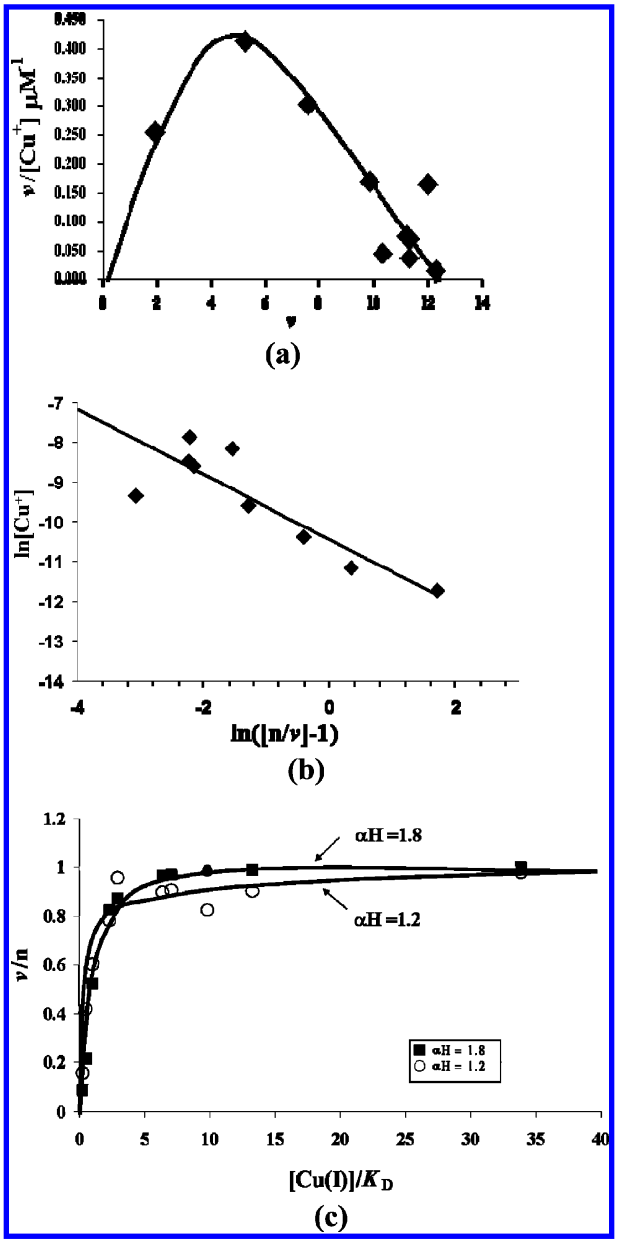

FIGURE 5: (a) Scatchard plot (eq 2) for the binding of ascorbate-reduced copper ions to apo-BCW1 V322E E343D with the His tag. (b) Linear Hill plot of eq 1. (c) Effect of the Hill constant α_H on the fractional saturation curve and comparison with experiment (○, $\alpha_H = 1.2$; ■, $\alpha_H = 1.8$).

plot (panel a), the number of Cu(I) binding sites n was deduced to be 12 ± 1, and the Hill constant α_H was ~1.8. The Hill plot (panel b) yielded an α_H of ~1.2 and a value of ~29.1 μM for the Cu(I) dissociation constant K_D. The lower Hill constant is consistent with the tighter Cu(I) binding to the apo-BCW1. Again, the fractional saturation data are in good agreement with the theoretical curves calculated for an α_H of either 1.8 or 1.2, as shown in Figure 5c. If the Cu(I) titration was conducted on the apo-BCW1 with the poly-His tag removed, the number of Cu(I) binding sites was determined to be 9 ± 2.

The apparent stepwise dissociation constant determined for the BCW1−Cu(I)$_n$ complex was about 10-fold lower when ascorbate was used as a reductant to generate Cu(I) from Cu(II). This outcome is to be expected since Cu(I) is known to interact more strongly with DTT than ascorbate

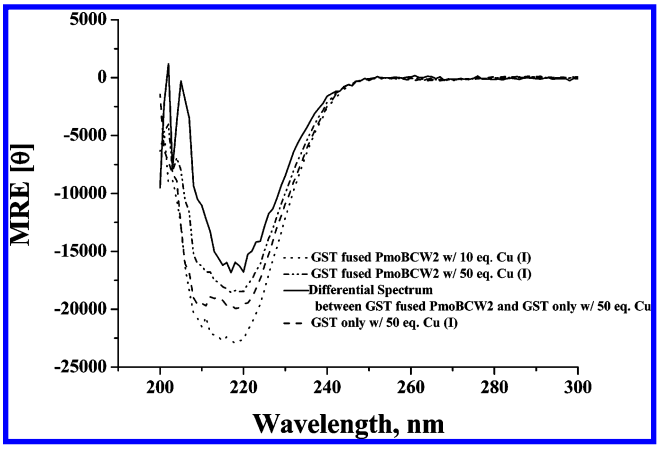

FIGURE 6: Binding of Cu(I) to the GST-fused PmoB aqueous domain apo-BCW2.

(*30*). A higher Cu(II)/DTT concentration is required to obtain the same activity of Cu(I) in the solution at equilibrium, thus the higher apparent K_D in the case of DTT (370 μM) relative to ascorbate (29.1 μM). Within the framework of the simple model used here to describe the complex multiple equilibria, we expect also a higher degree of cooperativity in the Cu(I) binding (α_H) with the larger Cu(I) dissociation constant K_D.

The Chan laboratory has previously argued on the basis of spectroscopic data that pMMO in *M. capsulatus* (Bath) as isolated contains ca. nine reduced Cu ions (dubbed E-clusters) (*20*, *21*). Moreover, these workers have suggested that these Cu ions reside in the water-exposed subdomains of the PmoB subunit (*3*, *22*). These earlier suggestions are now supported by the present experiments on BCW1. Regardless of the details of the method used to assay the Cu(I)-binding equilibrium and the simplicity of the model to interpret the Cu(I) titration data, essentially the same conclusions were obtained; apo-BCW1 can take up ca. 10 Cu(I) ions cooperatively to form a tight multiple-Cu(I) complex.

The β-Sheet Conformation of GST-Fused BCW1 Is Also Strongly Dependent on Cu(I). To further confirm that the C-terminal subdomain of the PmoB subunit has strong affinity toward Cu(I) ions, we have inserted the sequence corresponding to PmoB amino acid residues 282−414 (BCW2) into the GST-containing vector pGEX-5X-1, transformed the recombinant vector to *E. coli* BL21 (DE3), and obtained GST-fused BCW2 after the addition of IPTG. We detected no mutation within the apo-BCW2, and the corresponding GST-fused apoproteins were no longer overexpressed as an inclusion body, but were soluble in the cytosol of the *E. coli*. Accordingly, it was possible to simplify the procedure for the preparation of the overexpressed proteins.

We exploited the same procedure that we used for poly-His-tagged fused apo-BCW1 to incorporate DTT-reduced Cu(II) ions into the GST-fused apo-BCW2 subdomain. Again, from the CD spectra (Figure 6), we observed an increase of the β-structure feature at 218 nm as the Cu(I) ion content was increased from 10 to 50 equiv with respect to the concentration of the GST-fused BCW2. As a control, there was no strong conformational change observed for the GST protein alone in the presence of Cu(I) ions. The GST revealed only the standard α-helix structural feature, with the CD appearing at 210 and 218 nm (data not shown). The changes observed for the MRE [θ] of GST upon the addition

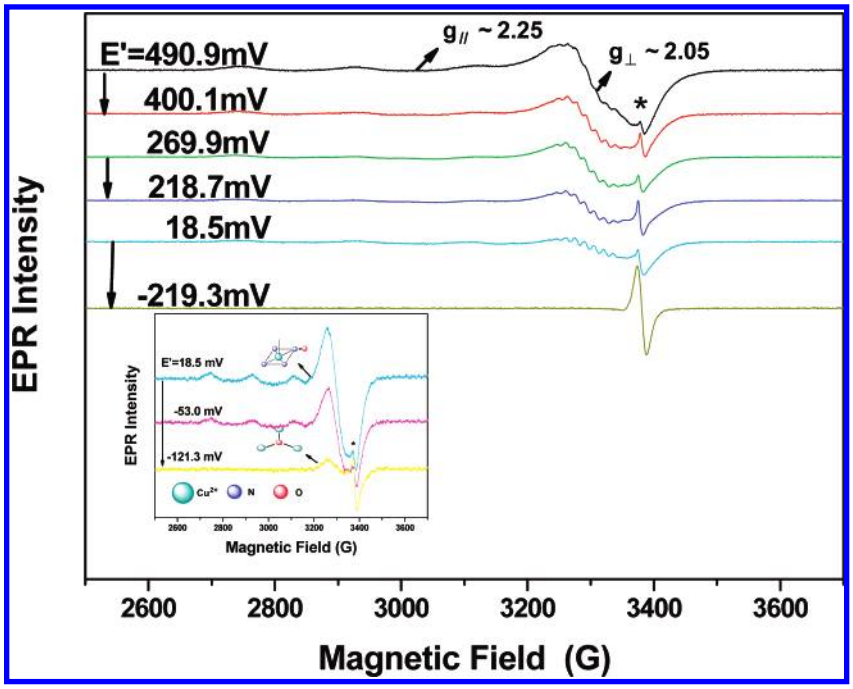

FIGURE 7: EPR (4 K) of the copper centers of pMMO samples poised at varying cell potentials by varying amounts of sodium dithionite in an anaerobic electrochemical cell in the presence of redox mediators at room temperature. Potentials are measured relative to SHE. Spectra were recorded (1) at +218.7 and +269.9 mV, obtained after purging with pure dioxygen for 1/2 h, where the EPR intensity corresponds to 3.72 and 4.86 Cu(II) ions per protein, respectively, and the spectra consist of the superposition of type 2 Cu(II) signals from 2−3 oxidized copper ions per protein from the E-clusters, together with the type 2 Cu(II) and trinuclear Cu(II) signals from the C-clusters (see the text), and (2) at +400.1 and +490.9 mV, obtained after purging with pure dioxygen for 8 h, where the EPR intensity corresponds to 6.51 and 9.87 Cu(II) ions per protein, respectively, indicating an additional 3−5 type 2 Cu(II) ions contributing from the E-clusters, or a total of 8 E-cluster copper ions per protein. The spectrum recorded at −219.3 mV gives the baseline, where essentially all the copper centers are reduced, except for the signals originating from free radicals associated with the dithionite and the redox mediators (identified by the asterisk at $g \approx 2.002$). Inset: spectra of the C-clusters of pMMO in purified pMMO-enriched membranes observed at +18.5, −53.0, and −121.3 mV.

of $CuSO_4$ in the presence of 10−50 equiv of DTT were also negligibly small. Thus, the folding of GST was not affected by the presence of Cu(I). Evidently, the fusion of GST to the BCW subdomain does not perturb the secondary structure or the tertiary fold of the subdomain that binds Cu(I) to stabilize its secondary structure.

As a followup, we also recorded the difference spectrum between GST-fused BCW2 and GST alone in the presence of 50 equiv of Cu(I) ions (MRE $[\theta] = -16\,000$ (deg·cm^2)/(dmol·residue)) at 218 nm (Figure 6). This difference spectrum should correspond to the CD spectrum of the Cu(I)-bound BCW2 subdomain, which in turn should be similar to the limiting spectrum obtained upon the Cu(I) titration on the secondary structure of the BCW1 V322E E343D subdomain, and indeed it was. Thus, there is no question that BCW1 is a Cu(I)-binding domain.

Redox Potential(s) of the E-Cluster Copper Ions in pMMO. The strong affinity of the BCW1 subdomain for Cu(I) and the weak binding of Cu(II) demonstrated in this study are tantamount to a high redox potential(s) for these copper ions when they are bound to the protein. Earlier work from the Chan laboratory has shown that when the pMMO in pMMO-enriched membranes is turned over by dioxygen in the absence of hydrocarbon substrate, only the catalytic copper sites (C-clusters) are oxidized according to the EPR and Cu Kα-edge X-ray absorption spectroscopy (*20*, *21*). The E-cluster copper ions remain reduced (Cu(I)). These E-cluster copper ions in the holoprotein are inert toward direct oxidation by molecular oxygen. The Cu(I) ions associated with the recombinant BCW1 subdomain exhibit a similar lack of reactivity toward dioxygen.

To demonstrate further direct correspondence between the copper ions bound to the recombinant BCW1 subdomain and the copper ions associated with the E-cluster-binding domain of pMMO in the membrane, we have carried out potentiometric titrations of pMMO in the purified pMMO-enriched membranes to determine the redox potential(s) of these copper ions. Recently, we reported redox potentiometry/EPR experiments on the C-cluster copper centers by poising pMMO-enriched membranes in an electrochemical cell at potentials ranging from +120 to −200 mV versus SHE (*17*). From these experiments, the midpoint potentials of the type 2 center and the trinuclear copper clusters were determined to be ca. −50 and −100 mV, respectively, versus SHE. We have now extended the measurements to high potentials where copper ions with higher redox potentials would be oxidized and become discernible in low-temperature EPR.

When pMMO-enriched membranes were purged with pure dioxygen for prolonged periods and incubated in the electrochemical cell at potentials above 200 mV, additional intensity became evident in the EPR spectrum that could not be attributed to the C-cluster copper ions. (The EPR of the type 2 Cu(II) center appears at $g_{av} \approx 2.12$, with Cu hyperfine in the parallel region ($g_{||} = 2.24$) and ^{14}N superhyperfine in the perpendicular region ($g_{\perp} = 2.059$); the EPR of the trinuclear Cu(II) cluster is depicted by an almost featureless isotropic signal centered at $g \approx 2.1$ (*18*, *21*).). The EPR spectrum is now augmented by a second type 2 Cu(II) signal,

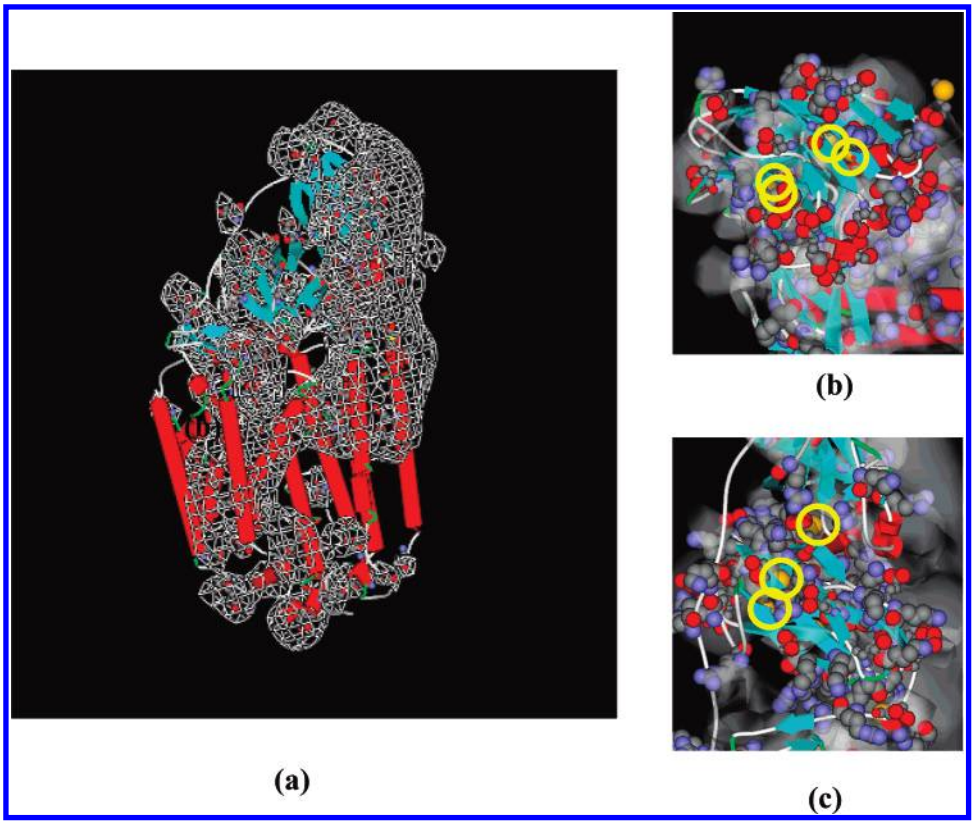

FIGURE 8: (a) Ribbon diagram of the crystal structure of the pMMO monomer (PmoABC, PDB code 1YEW1) from *M. capsulatus* (Bath) showing the negative electrostatic potential and the contour of the isopotential surfaces with an isovalue of −1 (white line). (b) Distribution of the acidic residues (red balls for oxygen atoms), basic residues (blue balls for nitrogen atoms), and methionines (yellow circles) in the C-terminal subdomain of PmoB. (c) Distribution of acidic residues and basic residues in the N-terminal subdomain of PmoB.

indicating onset of the oxidation of the E-cluster copper ions (Figure 7). The E-cluster type 2 Cu(II) EPR signals are readily distinguished from the type 2 Cu(II) signal elicited from the C-clusters, because it does not exhibit the ^{14}N superhyperfine structure of the latter in the perpendicular region (see Figure 7, inset (spectra recorded at cell potentials of −121.3, −53.0, and +18.5 mV versus SHE)).

When the pMMO-enriched membranes were purged with pure dioxygen for 1/2 h, only 2−3 of these E-cluster copper ions were oxidized (1.72 additional copper ions per protein at $E' = +218.7$ mV and 2.86 additional copper ions at $E' = +269.9$ mV). When it was purged for a period of 8 h, 2 more copper ions were observed at $E' = +400.1$ mV, and up to 5 additional copper ions were observed at $E' = +490.9$ mV. Thus, the apparent redox potentials of these E-cluster copper ions range from +200 to +490 mV versus SHE, consistent with their propensity to stay Cu(I) in the enzyme. The EPR intensity now accounts for a total of 12 copper ions per protein molecule. Since the EPR included 4 Cu(II) ions from the C-clusters at the outset, at least 8 Cu(II) ions have been elicited from the E-clusters under the high cell potentials employed in these experiments.

It would seem that these redox potentiometry data, taken in conjunction with the Cu(I)-binding results on the BCW1 and BCW2 subdomains described earlier, provide compelling evidence that the E-cluster copper ions of pMMO are located in the C-terminal subdomain of PmoB.

DISCUSSION

We have cloned and overexpressed in *E. coli* the two aqueous-exposed subdomains (residues 54−178, 257−394, and 282−414) of the 45 kDa subunit (PmoB) in pMMO from *M. capsulatus* (Bath) and have examined their secondary structures and copper ion binding properties. The recombinant N-terminal domain (residues 54−178) folds into a stable β-sheet structure, and we have obtained no evidence that it binds either Cu(II) or Cu(I) ions. In contrast, the recombinant C-terminal subdomain (257−394 and 282−414) exhibits a strong affinity for Cu(I) ions. It seems to behave like a Cu(I) sponge, with a capacity for ca. 10 Cu(I) ions. The binding of successive Cu(I) ions proceeds with strong positive cooperativity. The secondary structure of this domain is also strongly dependent on the Cu(I) concentration. Only weak Cu(II) binding was noted for this subdomain.

The N-terminal and C-terminal aqueous-exposed subdomains are the only regions in the three-dimensional fold of the pMMO where presumably NADH or other water-soluble reductants can access the E-clusters in the cytosol to transfer reducing equivalents into the pMMO after these copper ions become oxidized during turnover. It is known that pMMO loses its NADH-driven activity when the E-cluster copper ions are stripped off, although the enzyme can still turn over with duroquinol as a reductant (*2*, *13*, *31*).

To understand why the PmoB C-terminal subdomain exhibits the observed strong preference for Cu(I) ions, we have subjected the published crystal structure of one of the monomers (PDB code 1YEW) (*7*) to electrostatic potential calculations. DelPhi default charge and size software provided by Discovery Studio 1.5 (Accelrys Software Inc.) (*32*, *33*) was used as the template to assign the default charge and radii for the pMMO molecule (PmoABC). These calculations showed that the C-terminal subdomain of PmoB

Table 1: Number of Cysteines (C), Aspartic Acids (D), Glutamic Acids (E), Histidines (H), Lysines (K), Methionines (M), and Arginines (R) in the pMMO Subunits (PmoABC) and the PmoB Water-Exposed Subdomains BNW, BCW1, and BCW2

amino acid	PmoA1	PmoB1	PmoC1	BNW	BCW1	BCW2
C	1	0	1	0	0	0
D	8	24	7	4	12	14
E	7	21	15	10	7	6
H	5	7	5	3	1	1
K	3	19	6	9	5	3
M	11	16	5	4	4	3
R	12	25	8	7	9	9

generates a negative electrostatic potential at the subdomain surface, and the contour of the isopotential surfaces with an isovalue of −1 coincides more or less with this surface (Figure 8a). This result is consistent with the fairly uniform distribution of −1 negative charges in essential contact with the aqueous interface throughout the subdomain (Figure 8b). There are many Asp and Glu residues associated with the C-terminal subdomain (Table 1). In the two overexpressed aqueous subdomains BCW1 V322E E343D and BCW2, there are 19 and 20 acidic amino acid residues, respectively. Examination of the primary sequences of these peptides indicates that there are insufficient positively charged residues (14 Lys and Arg residues in the case of BCW1 and 12 in the case of BCW2) to balance the negative charges in the apo-BCW subdomain. Thus, the observed stabilization of the β-sheet structure by Cu(I) binding in BCW1 and BCW2 is understandable within the context of charge balance. Of course, the high redox potentials observed for these copper ions also argue for other ligands such as His and Met with the ligand geometry or environment to favor Cu(I) coordination in each case. While these Asp and Glu residues must account for the negative charges responsible for the Cu(I) binding, the distribution or positioning of these other copper ligands must also be favorably disposed to facilitate the cooperative binding of the Cu(I) ions. Figure 8b shows the distribution of Asp, Glu, His, Lys, and Arg as well as the four Met residues that form part of the C-terminal subdomain.

In the pMMO, the N-terminal subdomain is sandwiched between the membrane interface and the C-terminal domain (Figure 8a). Although this subdomain also includes many Asp and Glu residues (Figure 8c), these residues are buried and more shielded electrostatically from the solvent. These acidic residues are also more likely to interact with the basic residues in the subdomain. There are 16 Lys and Arg residues versus 14 acidic residues in the BNW peptide so that there is almost charge balance in this subdomain (Table 1). Consistent with this, in the electrostatic analysis summarized in Figure 8a, the isopotential contour corresponding to the isovalue of −1 lies below or under the subdomain surface. Accordingly, the N-terminal subdomain is most likely a structural domain, providing a structural scaffold to orient the C-terminal subdomain so that the surfaces bearing the negatively charged Asp and Glu in the C-terminus are facing the aqueous solution.

Although the intrinsic affinity of the C-terminal subdomain for Cu(I), as manifested by the stepwise dissociation constant K_D of 29.1 or 370 μM, is not particularly strong, the cooperativity observed for the binding of Cu(I) to the apo-BCW ensures that the association of the bulk of the Cu(I) ions is extremely tight. This conclusion is evident from the fractional saturation curves highlighted in panel c of Figures 4 and 5. While the first Cu(I) ions that go on to the subdomain would not be strongly bound, on the average, they become more tightly bound as additional Cu(I) ions are associated. This finding clarifies why the Cu(I) ions remain associated with the protein when the pMMO is exposed to the relatively low Cu(I) medium in the cytosol and why the copper ions are readily lost during the purification process, particularly when they become oxidized. Because of the high stability of Cu(II) relative to Cu(I) in buffer, Cu(II) ions do not seem to be able to sustain the secondary structure of the C-terminal domain of PmoB as well as Cu(I).

Earlier work (*13*, *16*, *25*, *34*) has shown that pMMO could be purified with reasonable activity if the protein preparation and purification procedures are maintained under a reducing environment. Once the E-cluster Cu(I) ions are oxidized, the copper ions are readily dissociated from the E-cluster domain if they are not quickly re-reduced. Without the E-cluster Cu(I) ions, the enzyme cannot sustain NADH-driven pMMO activity (*2*, *4*, *13*). This explains why the preparations used in the X-ray structural analysis do not possess biochemical activity when NADH is used as the reductant (*7*). In fact, the procedures adopted by Lieberman and Rosenzweig (*7*) to purify the enzyme do not yield a preparation that supports biochemical activity, whether NADH or duroquinol is deployed as the reductant (*17*). In this preparation, the tricopper cluster that mediates O-atom transfer has also been stripped off during the harsh purification procedures used to obtain the protein for X-ray diffraction analysis (*17*).

The redox potential(s) of the E-cluster copper ions are atypically high. These copper ions stay reduced during the purification of the enzyme (*3*, *13*, *20*, *21*) if they are not stripped away during the process, and they remain reduced even when the active site copper ions or C-clusters are oxidized in the absence of hydrocarbon substrate. Under these circumstances, the transfer of reducing equivalents from the E-clusters to the C-clusters is thermodynamically uphill: the redox potential(s) of the E-cluster copper ions are significantly higher than the redox potential(s) of the C-cluster copper ions. In the presence of hydrocarbon substrate, on the other hand, the electrons from the E-cluster copper ions are rapidly transferred to the C-clusters following the hydroxylation of substrate (*3*, *21*). These observations suggest that the E-cluster and C-cluster domains of the enzyme are allosterically linked. Since the E-cluster copper ions evidently provide a buffer of reducing equivalents to reduce the active site copper ions upon completion of the hydroxylation of the substrate, the redox potential(s) of the E-clusters must be tightly coupled to this allosteric linkage. Conceivably, the redox potential of the E-cluster copper ions could be collectively tuned by global structural changes in the C-terminal subdomain, especially one that leads to enhanced exposure of the copper binding sites and increases the accessibility of the bound copper ions to the solvent. This scenario might provide a mechanism for thermodynamic control of the redox potential(s) of the E-cluster copper ions and a method of kinetic gating of the electron flow from the E-clusters to the C-clusters to facilitate re-reduction of the

copper ions at the catalytic site following the oxidative phase of the turnover cycle. Without this electron gating, the O-atom transfer would be aborted in favor of oxidase chemistry if the electron transfer is sufficiently rapid.

In summary, we have provided evidence that the C-terminal domain of PmoB in pMMO is a reservoir for Cu(I) with properties similar to those of the E-cluster copper ions in the intact holoenzyme. These findings argue in favor of the E-clusters as an integral component of pMMO, and these copper ions probably play an important function in the turnover of the enzyme.

ACKNOWLEDGMENT

We thank Dr. Michael K. Chan (Departments of Chemistry and Biochemistry at The Ohio State University) and Dr. Hoa H.-T. Nguyen (TransMembrane BioSciences, Pasadena, CA) for a number of helpful discussions.

REFERENCES

1. Murray, E. P., Tsai, T., and Barnett, S. A. (1999) A direct-methane fuel cell with a ceria-based anode, *Nature 400*, 649−651.
2. Basu, P., Katterle, B., Andersson, K. K., and Dalton, H. (2003) The membrane-associated form of methane mono-oxygenase from *Methylococcus capsulatus* (Bath) is a copper/iron protein, *Biochem. J. 369*, 417−427.
3. Chan, S. I., Chen, K. H. C., Yu, S. S. F., Chen, C. L., and Kuo, S. S. J. (2004) Toward delineating the structure and function of the particulate methane monooxygenase from methanotrophic bacteria, *Biochemistry 43*, 4421−4430.
4. Choi, D. W., Kunz, R. C., Boyd, E. S., Semrau, J. D., Antholine, W. E., Han, J. I., Zahn, J. A., Boyd, J. M., de la Mora, A. M., and DiSpirito, A. A. (2003) The membrane-associated methane monooxygenase (pMMO) and pMMO-NADH:quinone oxidoreductase complex from *Methylococcus capsulatus* bath, *J. Bacteriol. 185*, 5755−5764.
5. Kao, W. C., Chen, Y. R., Yi, E. C., Lee, H., Tian, Q., Wu, K. M., Tsai, S. F., Yu, S. S. F., Chen, Y. J., Aebersold, R., and Chan, S. I. (2004) Quantitative proteomic analysis of metabolic regulation by copper ions in *Methylococcus capsulatus* (Bath), *J. Biol. Chem. 279*, 51554−51560.
6. Kitmitto, A., Myronova, N., Basu, P., and Dalton, H. (2005) Characterization and structural analysis of an active particulate methane monooxygenase trimer from *Methylococcus capsulatus* (Bath), *Biochemistry 44*, 10954−10965.
7. Lieberman, R. L., and Rosenzweig, A. C. (2005) Crystal structure of a membrane-bound metalloenzyme that catalyses the biological oxidation of methane, *Nature 434*, 177−182.
8. Murray, L. J., Garcia-Serres, R., Naik, S., Huynh, B. H., and Lippard, S. J. (2006) Dioxygen activation at non-heme diiron centers: Characterization of intermediates in a mutant form of toluene/o-xylene monooxygenase hydroxylase, *J. Am. Chem. Soc. 128*, 7458−7459.
9. Murrell, J. C., McDonald, I. R., and Gilbert, B. (2000) Regulation of expression of methane monooxygenases by copper ions, *Trends Microbiol. 8*, 221−225.
10. Myronova, N., Kitmitto, A., Collins, R. F., Miyaji, A., and Dalton, H. (2006) Three-dimensional structure determination of a protein supercomplex that oxidizes methane to formaldehyde in *Methylococcus capsulatus* (Bath), *Biochemistry 45*, 11905−11914.
11. Yu, S. S. F., Wu, L. Y., Chen, K. H. C., Luo, W. I., Huang, D. S., and Chan, S. I. (2003) The stereospecific hydroxylation of [2,2-$^2H_2$]butane and chiral dideuteriobutanes by the particulate methane monooxygenase from *Methylococcus capsulatus* (bath), *J. Biol. Chem. 278*, 40658−40669.
12. Zheng, H., and Lipscomb, J. D. (2006) Regulation of methane monooxygenase catalysis based on size exclusion and quantum tunneling, *Biochemistry 45*, 1685−1692.
13. Yu, S. S. F., Chen, K. H. C., Tseng, M. Y. H., Wang, Y. S., Tseng, C. F., Chen, Y. J., Huang, D. S., and Chan, S. I. (2003) Production of high-quality particulate methane monooxygenase in high yields from *Methylococcus capsulatus* (Bath) with a hollow-fiber membrane bioreactor, *J. Bacteriol. 185*, 5915−5924.
14. Lipscomb, J. D. (1994) Biochemistry of the soluble methane monooxygenase, *Annu. Rev. Microbiol. 48*, 371−399.
15. Kopp, D. A., and Lippard, S. J. (2002) Soluble methane monooxygenase: activation of dioxygen and methane, *Curr. Opin. Chem. Biol. 6* (5), 568−576.
16. Nguyen, H. H. T., Elliott, S. J., Yip, J. H. K., and Chan, S. I. (1998) The particulate methane monooxygenase from methylococcus capsulatus (Bath) is a novel copper-containing three-subunit enzyme−Isolation and characterization, *J. Biol. Chem. 273*, 7957−7966.
17. Chan, S. I., Wang, V. C.-C., Lai, J. C.-H., Yu, S. S.-F., Chen, P. P.-Y., Chen, K. H.-C., Chen, C.-L., and Chan, M. K. (2007) Redox potentiometry studies of particulate methane monooxygenase: Support for a trinuclear copper cluster active site, *Angew. Chem., Int. Ed. 46*, 1992−1994.
18. Hung, S. C., Chen, C. L., Chen, K. H. C., Yu, S. S. F., and Chan, S. I. (2004) The catalytic copper clusters of the particulate methane monooxygenase from methanotrophic bacteria: Electron paramagnetic resonance spectral simulations, *J. Chin. Chem. Soc. 51*, 1229−1244.
19. Chen, P. P. Y., and Chan, S. I. (2006) Theoretical modeling of the hydroxylation of methane as mediated by the particulate methane monooxygenase, *J. Inorg. Biochem. 100*, 801−809.
20. Nguyen, H. H. T., Nakagawa, K. H., Hedman, B., Elliott, S. J., Lidstrom, M. E., Hodgson, K. O., and Chan, S. I. (1996) X-ray absorption and EPR studies on the copper ions associated with the particulate methane monooxygenase from *Methylococcus capsulatus* (Bath). Cu(I) ions and their implications, *J. Am. Chem. Soc. 118*, 12766−12776.
21. Chen, K. H. C., Chen, C. L., Tseng, C. F., Yu, S. S. F., Ke, S. C., Lee, J. F., Nguyen, H. T., Elliott, S. J., Alben, J. O., and Chan, S. I. (2004) The copper clusters in the particulate methane monooxygenase (pMMO) from *Methylococcus capsulatus* (Bath), *J. Chin. Chem. Soc. 51*, 1081−1098.
22. Vinchurkar, M. S., Chen, K. H. C., Yu, S. S. F., Kuo, S. J., Chid, H. C., Chien, S. H., and Chan, S. I. (2004) Polarized ATR-FTIR spectroscopy of the membrane-embedded domains of the particulate methane monooxygenase, *Biochemistry 43*, 13283−13292.
23. Lieberman, R. L., Shrestha, D. B., Doan, P. E., Hoffman, B. M., Stemmler, T. L., and Rosenzweig, A. C. (2003) Purified particulate methane monooxygenase from *Methylococcus capsulatus* (Bath) is a dimer with both mononuclear copper and a copper-containing cluster, *Proc. Nat. Acad. Sci. U.S.A. 100*, 3820−3825.
24. Balasubramanian, R., and Rosenzweig, A. C. (2007) Structural and mechanistic insights into methane oxidation by particulate methane monooxygenase, *Acc. Chem. Res. 40*, 573−580.
25. Semrau, J. D., Zolandz, D., Lidstrom, M. E., and Chan, S. I. (1995) The role of copper in the Pmmo of *Methylococcus capsulatus* Bath−a structural vs catalytic function, *J. Inorg. Biochem. 58*, 235−244.
26. Bradford, M. M. (1976) A rapid and sensitive for the quantitation of microgram quantities of protein utilizing the principle of protein-dye binding, *Anal. Biochem. 72*, 248−254.
27. Jensen, P. Y., Bonander, N., Horn, N., Tümer, Z., and Farvar, O. (1999) Expression, purification and copper-binding studies of the first metal-binding domain of Menkes protein, *Eur. J. Biochem. 264*, 890−896.
28. Cantor, R. C., and Schimmel, P. R., Eds. (1980) *Biophysical Chemistry, Part III*, W. H. Freeman and Co., New York.
29. Dutton, P. L. (1987) Redox potentiometry: Determination of midpoint potentials of oxidation-reduction components of biological electron-transfer systems, *Methods Enzymol. 54*, 411−435.
30. Krężel, A., Leśniak, W., Jeżowska-Bojczuk, M., Młynarz, P., Brasuň, J., Kozłowski, H., and Bal, W. (2001) Coordination of heavy metals by dithiothreitol, a commonly used thiol group protectant, *J. Inorg. Biochem. 84*, 77−88.
31. Shiemke, A. K., Cook, S. A., Miley, T., and Singleton, P. (1995) Detergent solubilization of membrane-bound methane monooxygenase requires plastoquinol analogs as electron-donors, *Arch. Biochem. Biophys. 321*, 421−428.
32. Klapper, I., Hagstrom, R., Fine, R., Sharp, K., and Honig, B. (1986) Focusing of electric fields in the active site of Cu-Zn superoxide dismutase: Effects of ionic strength and amino-acid modification, *Proteins 1*, 47−59.
33. Gilson, M., and Honig, B. (1987) Calculations of electrostatic potentials in an enzyme active site, *Nature 330*, 84−86.

34. Nguyen, H. H. T., Shiemke, A. K., Jacobs, S. J., Hales, B. J., Lidstrom, M. E., and Chan, S. I. (1994) The nature of the copper ions in the membranes containing the particulate methane monooxygenase from *Methylococcus capsulatus* (Bath), *J. Biol. Chem. 269*, 14995−15005.

BI700883G